Four Dimensional Spectral-Spatial Fat Saturation Pulse Design

Feng Zhao,* Jon-Fredrik Nielsen, and Douglas C. Noll

Purpose: The conventional spectrally selective fat saturation pulse may perform poorly with inhomogeneous amplitude of static (polarizing) field (B$_0$) and/or amplitude of (excitation) radiofrequency field (B$_1$) fields. We propose a four dimensional spectral-spatial fat saturation pulse that is more robust to B$_0$/B$_1$ inhomogeneity and also shorter than the conventional fat saturation pulse.
Theory: The proposed pulse is tailored for local B$_0$ inhomogeneity, which avoids the need of a sharp transition band in the spectral domain, so it improves both performance and pulse length. Furthermore, it can also compensate for B$_1$ inhomogeneity. The pulse is designed sequentially by small-tip-angle approximation design and an automatic rescaling procedure.
Methods: The proposed method is compared to the conventional fat saturation in phantom experiments and in vivo knee imaging at 3 T for both single-channel and parallel excitation versions.
Results: Compared to the conventional method, the proposed method produces superior fat suppression in the presence of B$_0$ and B$_1$ inhomogeneity and reduces pulse length by up to half of the standard length.
Conclusion: The proposed four dimensional spectral-spatial fat saturation suppresses fat more robustly with shorter pulse length than the conventional fat saturation in the presence of B$_0$ and B$_1$ inhomogeneity. **Magn Reson Med 72:1637–1647, 2014. © 2013 Wiley Periodicals, Inc.**

Key words: fat saturation; pulse design; spectral-spatial pulse; parallel excitation; B$_0$ inhomogeneity; B$_1$ inhomogeneity

INTRODUCTION

Fat suppression has been widely used in MRI to suppress undesired adipose tissue signals or prevent chemical shift artifacts. One popular method is fat sat(uration) (1), which uses a spectrally selective pulse to saturate and dephase fat spins preceding the actual imaging pulse sequence. Fat sat is compatible with most imaging sequences, but it is sensitive to amplitude of static (polarizing) field (B$_0$) and amplitude of (excitation) radiofrequency field (B$_1$) inhomogeneity. Another popular preparatory pulse for fat suppression is short T$_1$ inversion recovery pulse (2,3), which is based on the unique T$_1$ of fat. Although this method is immune to B$_0$ field inhomogeneity, it has many drawbacks, such as

long scan time, reduced signal-to-noise ratio of water signal, and altered T$_1$ contrasts. Instead of preparatory pulses, spectral-spatial (SPSP) pulse was proposed to selectively excite water tissue (4). This pulse specifies excitation profiles in both spatial and spectral domain, but it is subject to B$_0$ inhomogeneity and may have drawbacks like poor slice profile or long pulse length.

This article focuses on improving the fat sat method by minimizing the adverse effects of B$_0$ and B$_1$ inhomogeneity with short pulses. Our approach to solving this problem is to incorporate information of the three dimensional (3D) B$_0$ and B$_1$ fields into the pulse design to excite a four dimensional (4D) SPSP pattern. Morrell et al. proposed a similar idea using 3D SPSP pulse to excite 3D patterns (two spatial and one spectral dimensions) based on two dimensional (2D) field maps, to mitigate B$_0$ inhomogeneity problems for 2D water-only imaging or fat saturation (5), but this method has limited use for 3D imaging or interleaved multislice imaging where 3D field maps are typically needed. Moreover, the pulse length of this design was too long for steady-state imaging sequences, and it does not handle B$_1$ inhomogeneity. With the advent of parallel excitation, Heilman et al. proposed efficient pulses to uniformly saturate fat via multichannel transmitters by tuning the center frequency of each coil to match the variation of B$_0$ maps (6), but it is difficult for this approach to address complex B$_0$ patterns and to insure uniform tip angles. Recently, a parallel excitation pulse design for broadband slab selection with B$_1$ inhomogeneity correction (7) demonstrates the feasibility of addressing some simple spectral profiles by tailored SPSP pulses in 3D k-space ($k_x - k_y - k_z$). In addition, Malik et al. proposed a water selective imaging method using parallel excitation to achieve more complex spectral profiles with SPSP pulses that are based on weighted binomial pulse trains in $k_z - k_f$ of k-space (8). However, absence of traversing within $k_x - k_y$ may lead to incomplete B$_0$/B$_1$ compensation in the transverse plane and thus makes the results highly dependent on the B$_0$ shimming and configurations of transmit coils.

In this article, we propose to tackle this problem by designing a 4D SPSP fat sat pulse that is tailored for B$_0$ and B$_1$ inhomogeneity of the 3D space. The proposed method avoids the need of a sharp transition band in the spectral domain by exploiting the spatial variations of center frequencies, so it can achieve better performance with even shorter pulse length than the standard fat sat pulse. Both single channel excitation and parallel excitation versions have been developed. This saturation pulse is numerically computed with an iterative algorithm composed of a small-tip angle approximation design and an automatic rescaling step. The proposed method is compared with the conventional fat sat pulse in phantom experiments and in vivo experiments on 3T

scanners for both the single channel excitation and the parallel excitation versions.

THEORY

We propose a 4D SPSP (1D spectral and 3D spatial) fat sat pulse design with the option of incorporating parallel excitation. The pulse is tailored to match B_0 and B_1 variations of the specified 3D space. It has been shown in (9) that small-tip-angle (STA) approximation can be valid for 90° designs except for a scaling factor. So, we propose a two-step design: using STA approximation to determine the pulse "shape" and then automatically computing the pulse "amplitude".

Beyond the robustness to B_0 and B_1 inhomogeneity, the proposed method can also largely improve the pulse efficiency. With certain conditions satisfied, this seemingly harder pulse design actually needs similar or even shorter pulse length than the conventional spectral pulse. The conventional fat sat pulse needs to have a relatively rapid transition between the water and fat spectra to accommodate the B_0 inhomogeneity of the whole 3D volume; in contrast, the 4D SPSP fat sat pulse only needs to handle much narrower spectra of each local voxel, which can be achieved with smoother transition bands in the frequency domain. In other words, the proposed method makes the task in frequency domain easier than the conventional method, and therefore shortens the pulse length.

Figure 1 illustrates the difference between the 4D fat sat pulse and the conventional spectral pulse in the frequency domain, where three representative voxels that have different local off-resonance frequencies are shown as examples. The 4D fat sat pulse fits the spectra of the each voxel much better than the spectral pulse which can not accommodate the B_0 variations over the volume. Moreover, the 4D fat sat pulse has a much smoother transition in the spectral domain than the spectral pulse, which reduces the pulse length.

Step 1: Determine the "Shape"

With the STA approximation, the 4D excitation pattern model is described as follows:

$$m(x, y, z, f) = i\gamma m_0 \sum_r S_r(x, y, z) \int_0^T b_r(t) e^{i2\pi[(x,y,z,f)\cdot\mathbf{k}(t)]} dt$$

[1]

where (x, y, z) is the spatial coordinate, f is frequency, $m(x, y, z, f)$ is the 4D excitation pattern, γ is the gyromagnetic ratio, m_0 is the equilibrium magnetization magnitude, $S_r(x, y, z)$ is the B_1 map of the rth coil, $b_r(t)$ is the radiofrequency (RF) pulse of each coil, $r = 1, 2, \ldots, R$, R is the number of transmit coils, T denotes the pulse length, and $\mathbf{k}(t) = [k_x(t), k_y(t), k_z(t), k_f(t)]$ denotes the 4D excitation k-space trajectory. In particular, the excitation k-space trajectories are defined to be backward integrals as follows:
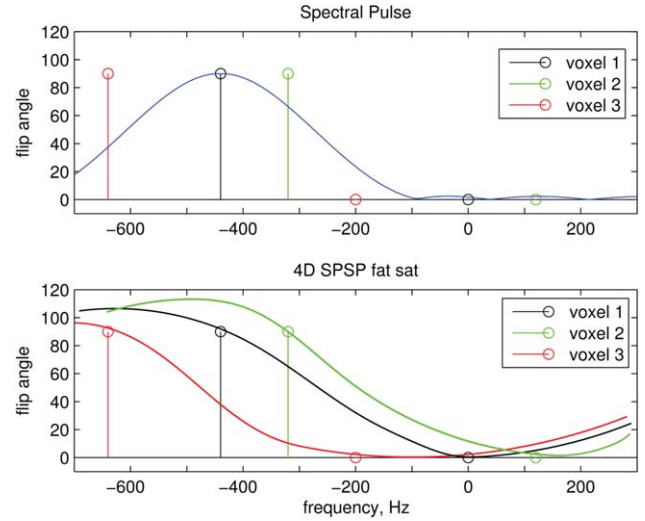

FIG. 1. Illustration of the frequency responses of the SLR fat sat pulse (top) and the 4D fat sat pulse (bottom) in the presence of B_0 inhomogeneity, where three voxels at different off-resonance frequencies are selected as examples. It shows that the 4D fat sat pulse suppresses fat without exciting water much more effectively with less sharp transition bands.

$$k_x(t) = -\frac{\gamma}{2\pi} \int_t^T G_x(\tau) d\tau, \quad k_f(t) = t - T$$

[2]

where x can also be y or z. The system Eq. 1 can be discretized as follows:

$$\mathbf{m} = \mathbf{A}_s \mathbf{b}$$

[3]

where $\mathbf{m}(N_s \times 1)$ is the vector that contains N_s samples of the 4D excitation pattern, $\mathbf{A}_s = [\mathbf{S}_1 \mathbf{A}\, \mathbf{S}_2 \mathbf{A} \ldots \mathbf{S}_R \mathbf{A}]$, $\mathbf{b} = [\mathbf{b}_1^T\, \mathbf{b}_2^T\, \ldots\, \mathbf{b}_R^T]^T$, $\mathbf{A}(N_s \times N_t)$ is system matrix that transform the RF pulse of each coil into the 4D pattern without considering the sensitivity map, i.e. $a_{ij} = i\gamma m_0 e^{i2\pi(x_i, y_i, z_i, f_i)\cdot\mathbf{k}(t_j)}$, $\mathbf{S}_r(N_s \times N_s)$ is a block diagonal matrix which contains the corresponding sensitivity maps of each coil repeated for each spectral sample, $\mathbf{b}_r(N_t \times 1)$ is the vector of samples of the RF pulse transmitted by each coil.

To do fat sat, the 4D target excitation pattern uniformly has 90° tip angles for the fat spectra and 0 for the water spectra in each voxel. To compensate for B_0 inhomogeneity, the positions of the fat and water bands of each voxel in the target pattern need to shift according to the 3D B_0 map. B_1 maps are input into Eq. 1 to compensate for B_1 inhomogeneity. In this 4D target pattern, most of the spectrum is a "don't care" region and can be masked out in the cost function to gain more degrees of freedom in the design; furthermore, the region outside the object can also be excluded from the target pattern.

With the system Eq. 3 and the target pattern, we design the pulses by iteratively optimizing a cost function that contains a target pattern fitting term and a regularization term for RF power penalization (9).

Furthermore, as the transverse phase of fat spins is not important, we apply magnitude least square optimization (10) to increase some degrees of freedom for the pulse design, where the final cost function can be described as:

$$\Phi(\boldsymbol{b}) = ||\boldsymbol{P} - |\boldsymbol{A_s b}|||_W^2 + \beta||\boldsymbol{b}||_2^2 \qquad [4]$$

where $\boldsymbol{P}$ ($N_s \times 1$) is the real valued 4D target pattern, $||\cdot||_W$ denotes the weighted L_2 norm that masks out the "don't care" region of the target pattern, and $\beta||\boldsymbol{b}||_2^2$ denotes the regularization term that penalizes the RF power and β is a scalar parameter. We use the approach proposed in Ref. (11) to solve this nonlinear optimization problem, which is to introduce another unknown vector $\boldsymbol{\phi}$ ($N_s \times 1$) to the cost function and alternately minimizes the new cost function Eq. 5 over $\boldsymbol{b}$ and $\boldsymbol{\phi}$:

$$\Phi(\boldsymbol{b}, \boldsymbol{\phi}) = ||\boldsymbol{P}.*e^{j\phi} - \boldsymbol{A_s b}||_W^2 + \beta||\boldsymbol{b}||_2^2 \qquad [5]$$

where $e^{j\phi}$ ($N_s \times 1$) denotes the vector with elements $e^{j\phi_i}, i = 1, 2, \ldots, N_s$, and ".*" denotes the element-by-element multiplication of two vectors. In particular, the step of updating $\boldsymbol{b}$ is implemented by using conjugate gradient algorithm (9) and nonuniform fast Fourier transform (12); $\boldsymbol{\phi}$ is updated in each iteration by taking the phase of the latest value of $\boldsymbol{A_s b}$, i.e., $\phi^{(n)} = \angle\{\boldsymbol{A_s b}^{(n)}\}$.

As the cost function Eq. 5 is nonconvex over $\boldsymbol{\phi}$, it needs to be initialized carefully to reach a good local minimum. There have been several different methods for the phase pattern initialization, such as zero phase and random phase (11), but none of them worked well in our implementation. Thus, we proposed a different initial phase pattern for this special problem, i.e., $\phi(x, y, z, f) = -2\pi f \frac{T}{2}$, and it worked much better than those conventional methods in our designs. Because the original target pattern with $\phi = 0$ is real and slowly varying over space, then the high energy parts of its k-space representation should be concentrated around the origin of the k-space; however, as the coverage of k_f is only over the nonpositive part, i.e., from $-T$ to 0, it can only cover half of the high energy parts of this target pattern in k-space. Hence, setting $\phi(x, y, z, f)$ to be $-2\pi f \frac{T}{2}$ solves this problem by shifting the target k-space by $T/2$ toward the negative part of k_f, which makes it possible to capture the most high energy parts of the target pattern in k-space. While this initial phase distribution works very well, it is not the only choice and may not be the best, as one may customize the variations of $\phi(x, y, z, f)$ over spatial locations for each frequency. Optimization of the initial phase configuration remains the subject of further research.

The gradient waveforms need to be set to traverse the 4D excitation k-space ($k_x - k_y - k_z - k_f$), which is achieved by repeating a 3D k-space trajectory ($k_x - k_y - k_z$) multiple times. We investigate two different types of 3D excitation k-space trajectories for traversing $k_x - k_y - k_z$: the "spoke" trajectory (also known as "fast-kz" trajectory) (13) and the "Spiral Nonselective (SPINS)" trajectory (14). The spoke trajectory is efficient when k_z needs to be sampled more

densely than $k_x - k_y$, such as 2D B_1 inhomogeneity compensation with slice selection (13). Thus, this trajectory seems suboptimal for our problem which has nearly isotropic variations in the 3D volume. In contrast, the SPINS trajectory, which is targeted for nonselective excitation, seems to be a better option in terms of efficiency. Moreover, as the SPINS trajectory traverses k-space center more densely and more slowly, specific absorption rate (SAR) and/or peak RF power could be smaller than those of the spoke trajectory. However, we still think it is arguable which one is better for this problem, because: (a) when using parallel excitation which usually only produces in-plane variations, the spoke trajectory may gain more efficiency than the SPINS trajectory, as k_z may need sampling more densely than $k_x - k_y$; (b) compared to SPINS trajectory, the spoke trajectory has fewer parameters and those parameters are more intuitive and more adjustable; (c) the eddy current effects of the spoke trajectory are less severe and more tractable than in the SPINS trajectory; (d) several methods have been proposed to optimize the spoke trajectory (15–18), whereas optimization of the SPINS trajectory remains much more challenging. We experimentally compared these two trajectories in terms of various practical specifications. Figure 2 shows examples of these two trajectories, respectively, where $k_x - k_y - k_z$ coverage is restricted such that k_f is sampled adequately densely.

Step 2: Determine the "Amplitude"

STA design only determines the pulse "shape," and the designed pulses still need to be properly rescaled to uniformly saturate the fat spins. To make the design practical for in vivo scans, we need an efficient and accurate way to determine the pulse "amplitude." Although existing large-tip parallel excitation design methods (19–21) are able to automate the design process, they would be too computationally intensive for this high dimensional problem. Thus, assuming the pulses designed in step 1 only need to be properly rescaled, we designed a simple iterative process to determine the pulse "amplitude":

---

1. A few, e.g., 50 pixels in the fat band that are best fit to the target pattern in step 1 are selected.
2. Apply the pulse $b^{(0)}$ designed by STA to the Bloch equation simulation and only compute for the points selected, and it then produces an average of tip angle $\theta^{(n)} - 90°|$. ($n = 0$)
3. while ($|\theta^{(n)} - 90°| > \epsilon$) {
   a. The pulse is updated to be $b^{(n+1)} = [\frac{1 + \sin(90° - \theta^{(n)})}{\sin(90°)}] \times b^{(n)}$;
   b. Repeat (2) for $b^{(n+1)}$ and get an average tip angle $\theta^{(n+1)}$;
   c. $n = n + 1$;
   }

When the pulses achieve uniform patterns for fat, this strategy is equivalent to the additive-angle method (19). As there is only one scalar to determine in this step, only a few pixels are sufficient; then the computation for Bloch equation simulation is very fast. Moreover, as 90°
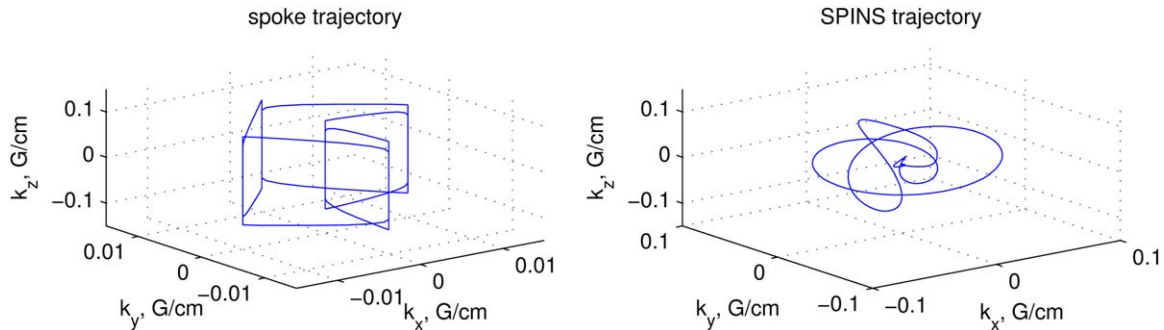
FIG. 2. Examples of the spoke trajectory (left) and SPINS trajectory (right) that are used in this work. [Color figure can be viewed in the online issue, which is available at wileyonlinelibrary.com.]

is relatively "small" in the large-tip excitation regime, this algorithm usually appears to converge in a few iterations. In practice, this step takes less than a second in Matlab (The Mathworks, Natick, MA).

METHODS

The proposed method is compared with the conventional spectrally selective fat sat pulse in a series of 3T experiments. In the phantom experiments, the spoke trajectory and the SPINS trajectory were both evaluated for single channel and parallel excitation versions. The proposed method was also applied to human knee imaging. All of the experiments were performed on two GE 3T scanners (GE Healthcare, Milwaukee, WI), using GE single channel transmit/receive head coils or an eight-channel custom parallel transmit/receive system (22,23). Table 1 summarizes all the experiments discussed in this paper.

Pulse Design

The proposed method is compared with the conventional spectrally selective fat sat pulse which is designed by the Shinnar-Le Roux (SLR) algorithm (24). The SLR fat sat pulse is 5 ms long and has a 400 Hz minimal phase passband for fat (center frequency is -440 Hz), which is typically used for 3T fat sat. For each pulse sequence, the amplitude of the pulse was properly adjusted to saturate the on-resonance fat spins.

The procedure of the proposed 4D fat sat pulse design is summarized in the flowchart in Figure 3. The steps in the blue box, which are for B_1 mapping and RF shimming, were only used in the parallel excitation experiments, as we found that B_1 inhomogeneity was acceptable in our 3T single channel excitation experi-

Table 1
The List of Experiments

	Objects	Equipment	Trajectories
Experiment 1	Phantom	Single channel excitation	Spoke
Experiment 2	Phantom	Single channel excitation	Spoke, SPINS
Experiment 3	Phantom	Parallel excitation	Spoke, SPINS
Experiment 4	Knees	Single channel excitation	SPINS

ments. For applications that are more susceptible to B_1 inhomogeneity, e.g., abdominal imaging in the presence of ascites (25), it may be necessary to incorporate B_1 maps in the design for single channel excitation experiments. In the parallel excitation experiments, the required eight-channel complex B_1 maps (B_1 magnitude and relative phase maps) were acquired by using a modified Bloch-Siegert B_1 mapping method (26–28) which produces both B_1 magnitude and phase maps with optimized signal-to-noise ratio. Moreover, RF shimming (29) was applied to achieve uniform excitation in the parallel excitation system, where the magnitude and phase of each coil of the transmit array were adjusted according to the complex B_1 maps. With the uniform excitation, we can obtain the B_0 maps from the phase difference of two Gradient echo images that have different echo times, and the echo time difference needs to be set such that the water and fat spins are in-phase, e.g., $\Delta T_E = 2.272$ ms on 3T scanners. The B_0 and B_1 maps are then put into the proposed 2-step 4D fat sat pulse design routine to get the desired fat sat pulses. Finally, the uniform excitation pulse and the designed 4D fat sat pulse are loaded onto the scanner to acquire the fat suppressed images.

Although this high dimensional design is computationally intensive, we still achieved a practical design time by using the following strategies. First, we coarsely sample the 4D SPSP domain, based on the following assumptions: (a) the target pattern varies smoothly with the B_0 and B_1 maps over the 3D spatial domain; (b) the spectra of fat and water in each voxel are relatively narrow and far apart. Second, most parts (usually 80–90%) of the 4D SPSP domain are "don't care" regions that can be masked out. Furthermore, as discussed in Theory section, the relatively small $k_x - k_y - k_z$ coverage and short k_f coverage, which, respectively, satisfies the sampling rate along k_f and shortens pulse length, also help to reduce the size of the system matrix. The voxel size of the target pattern and the corresponding B_0 and B_1 maps was around 1 cm^3, and the sampling rate in the frequency domain was about 20 Hz/point. The bandwidths of water and fat were set to be 40 and 80 Hz, respectively. The spoke trajectory samples 5 $k_x - k_y$ points as shown in Figure 2, where the locations of $k_x - k_y$ samples were empirically chosen to be uniform around the origin. The SPINS trajectory was designed according to the parameters suggested in (14). The maximal gradient
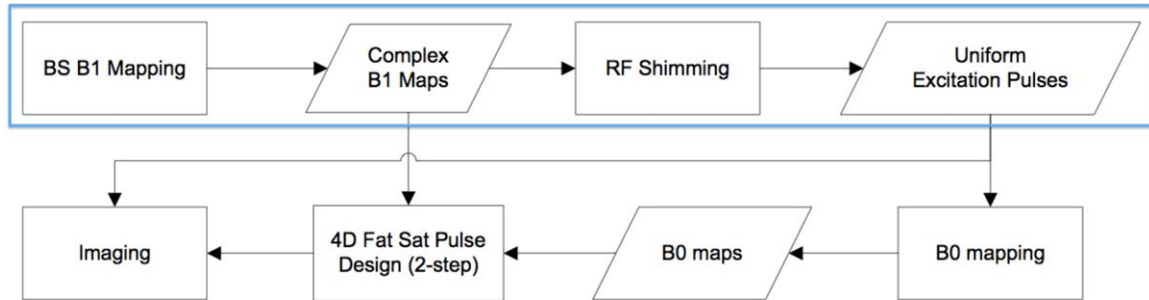
FIG. 3. The flowchart of the 4D fat sat pulse design and imaging procedure. The steps in the blue box were only used in parallel excitation experiments. [Color figure can be viewed in the online issue, which is available at wileyonlinelibrary.com.]

slew rate of both trajectories were driven towards the system limits, which is 180 $Tm^{-1}s^{-1}$. The sampling interval along k_f, i.e., the time for traversing $k_x - k_y - k_z$, was below 1 ms, keeping any possible aliases in frequency domain at least 1 kHz away from each other.

All of our pulse designs were implemented in Matlab 7.8 on a work station equipped with Intel Core2 Quad CPU Q9400 @ 2.66 GHz and 4 GB RAM, which takes about 1–2 min for the single channel excitation pulse and about 3–5 min for the parallel excitation pulse. The computation time would be acceptable in practice with a more efficient implementation and a more powerful computer.

Phantom Experiments with Single Channel Excitation

We then carried out two phantom experiments to test the single channel excitation version of the 4D fat sat pulse. The first phantom experiment (called "experiment 1" hereafter) compares the proposed method with the SLR fat sat pulse, and the second experiment (called "experiment 2" hereafter) studies the proposed method with different trajectories and pulse lengths. A cylindrical phantom filled with distilled water ($CuSO_4$ doped) and mineral oil was used for all those experiments.

In experiment 1, we designed a 4.8 ms 4D fat sat pulse for a $14 \times 14 \times 6$ cm^3 axial slab of the phantom based on

its multislice B_0 maps (Fig. 4). The spoke trajectory was applied with sampling period along k_f of 0.6 ms and 9 k_f samples. No RF power penalization was applied. It is compared with the 5 ms SLR fat sat pulse. We implemented the standard fat saturation scheme where the fat sat pulse is followed by a multislice 2D interleaved spiral-out readout. To measure the residual M_z, we play each sequence twice (turn fat sat on or off) with the same parameters: $T_E = 6ms$, $T_R = 15s$, $FOV = 14cm$, slice thickness $= 4mm$, 15 slices, 4 interleaves, and reconstruction size is 64×64. A long T_R is used so that we could approximately calculate the absolute value of the normalized residual M_z by taking the ratio: $|M_z| \approx |$the fat saturated image$|/|$the nonfat-sat image$|$.

In experiment 2, we applied the 4D fat sat pulse with the spoke and SPINS trajectories as well as the SLR fat sat pulse on the same phantom. A 3D spoiled gradient-echo sequence (SPGR) with field of view $14 \times 14 \times 7$ cm^3 was applied to acquire the B_0 map (Fig. 6). We then designed four different 4D fat sat pulses, which are 4.8 or 2.5 ms 4D fat sat pulses with a spoke or SPINS trajectory. The two 4.8 ms pulses both sample k_f nine times, whereas the two 2.5 ms pulses sample k_f five times. Among these four pulses, only the 2.5 ms spoke pulse used RF power penalization. The pulses were tested with 3D SPGR sequences that have a 7 cm slab-select
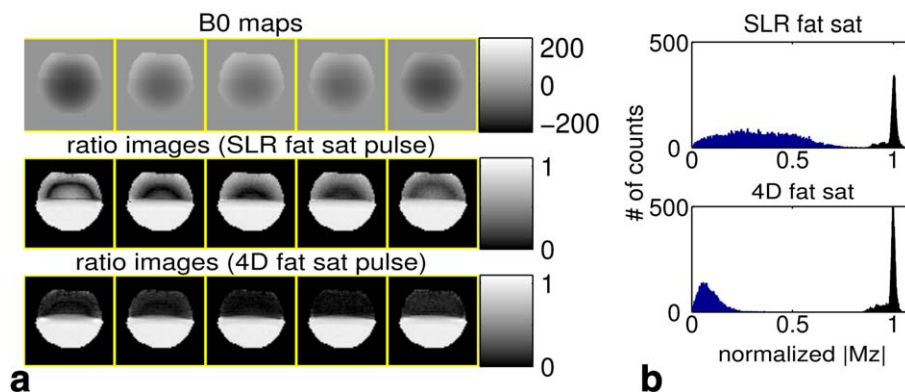

FIG. 4. The B_0 maps and the results of experiment 1. **a:** Top: the B_0 maps (in Hz); Middle and bottom: the ratio images by the SLR fat sat pulse (middle) or the 4D fat sat pulse (bottom), where the ratio images are the ratio between the images with fat sat and the ones without fat sat; Note that oil is on the top and water is the bottom in each image, and every third of the axial slices is shown. **b:** The histograms (200 bins) of the water (black) and fat (blue) M_z according to the ratio images of all the slices, where the SLR fat sat pulse (top) is compared with the 4D fat sat pulse (bottom). [Color figure can be viewed in the online issue, which is available at wileyonlinelibrary.com.]

excitation and spin-warp readout, and the imaging parameters were: $T_R = 213\text{ms}$, $\text{FOV} = 14 \times 14 \times 7\text{cm}^3$, and data size $= 64 \times 64 \times 15$. For each pulse, a pair of 3D images were acquired with fat sat on or off.

Phantom Experiments with Parallel Excitation

The parallel excitation version of 4D fat sat pulses was tested on the same phantom, which is called "experiment 3" hereafter. Due to partial amplifier failure, we only used four of the eight parallel excitation coils for transmission whereas all eight parallel receive channels were used. 2D B_1 maps of the parallel transmit channels were acquired and shown in Figure 7. They were then stacked up to form the 3D B_1 maps, assuming uniform B_1 field along z. We then designed the complex weights for uniform excitation using RF shimming. Then, we acquired the 3D B_0 map (Fig. 7) using a 3D SPGR sequence with field of view $14 \times 14 \times 10.5$ cm^3, where a 5.9 cm thick axial slab was used for the pulse design.

We designed 4.8 or 2.7 ms 4D fat sat pulses with a spoke or SPINS trajectory, each of which used the "heuristically optimized" k-space trajectory: the 4.8 ms spoke trajectory samples k_f every 0.6 ms for nine times; the 4.8 ms SPINS trajectory samples k_f about every 1 ms for five times; the 2.7 ms SPINS trajectory samples k_f every 0.54 ms for five times. We did not test spoke pulses shorter than 4.8 ms, which is discussed in Discussion section. All the designs required RF power penalization to satisfy the power limit of the amplifiers. The SLR fat sat pulse with the weights for uniform excitation was also applied for comparison.

All the pulses were tested with 3D SPGR sequences that have a nonselective excitation and spin-warp readout, and the imaging parameters were: $T_R = 80\text{ms}$, $\text{FOV} = 14 \times 14 \times 10.5\text{cm}^3$, and data size $= 64 \times 64 \times 48$. For each pulse, a pair of 3D images were acquired with fat sat

on or off. Note that, the raw data were eight-channel parallel imaging data, and they were combined using the receive side B_1 shimming according to the receive sensitivity maps acquired off-line. The results shown in Result section are all combined images.

In Vivo Experiments with Single Channel Excitation

The 4D fat sat pulse with single channel excitation was demonstrated in a knee imaging experiment (called "experiment 4" hereafter). A healthy volunteer participated with approval by the Institutional Review Board of the University of Michigan, after providing informed consent. To insure safety, a relatively long repetition time was used and global SAR was monitored during the experiments. As head coil may underestimate the global SAR for knee imaging, we kept the monitored global SAR values on the scanner below 5% of the relevant limit. We used the 2.5 ms 4D fat sat pulse with SPINS trajectory which worked best in the single channel excitation phantom experiments and compared it with the 5 ms SLR fat sat pulse. The 3D B_0 map of a $28 \times 28 \times 6.5$ cm^3 ($64 \times 64 \times 13$) axial slab of human knees was acquired with a 3D SPGR sequence, and Figure 8 shows two representative slices. No penalization was put on peak RF power. Both of the fat sat pulses were tested with 3D SPGR sequences that have a slab-select excitation and spin-warp readout, and the imaging parameters were: $T_R = 91\text{ms}$, $\text{FOV} = 28 \times 14 \times 6.5\text{cm}^3$, data size $= 256 \times 128 \times 13$.

RESULTS

Phantom Experiments with Single Channel Excitation

The results (every third slice) of experiment 1 are shown in Figure 4 where 4D fat sat pulse is compared with SLR
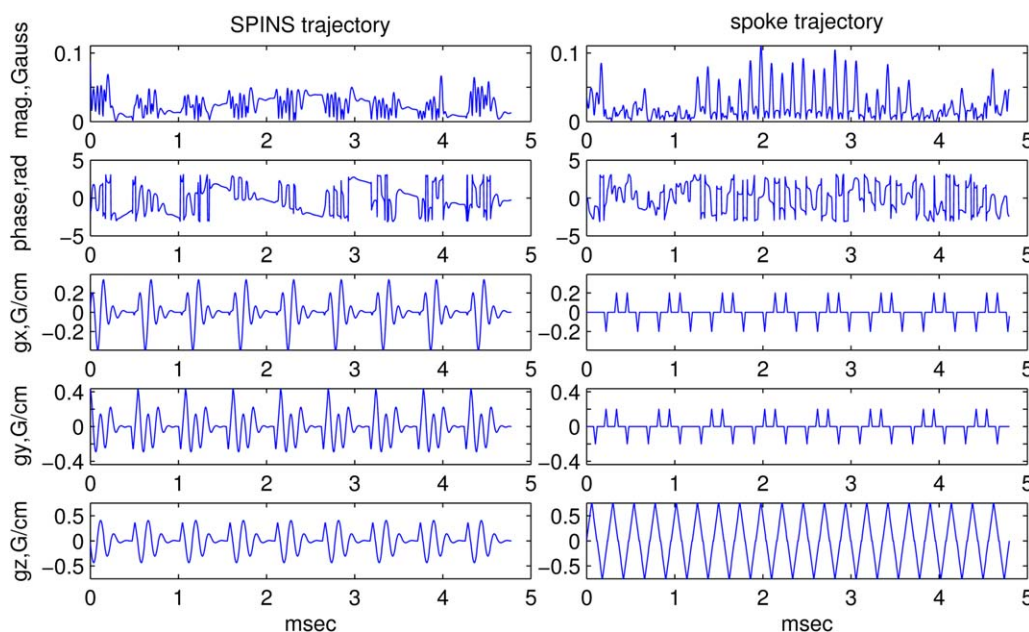

FIG. 5. Examples of the designed 4D fat sat pulses: 4.8 ms 4D fat sat pulse with SPINS trajectory (left); 4.8 ms 4D fat sat pulse with spoke trajectory (right). [Color figure can be viewed in the online issue, which is available at wileyonlinelibrary.com.]
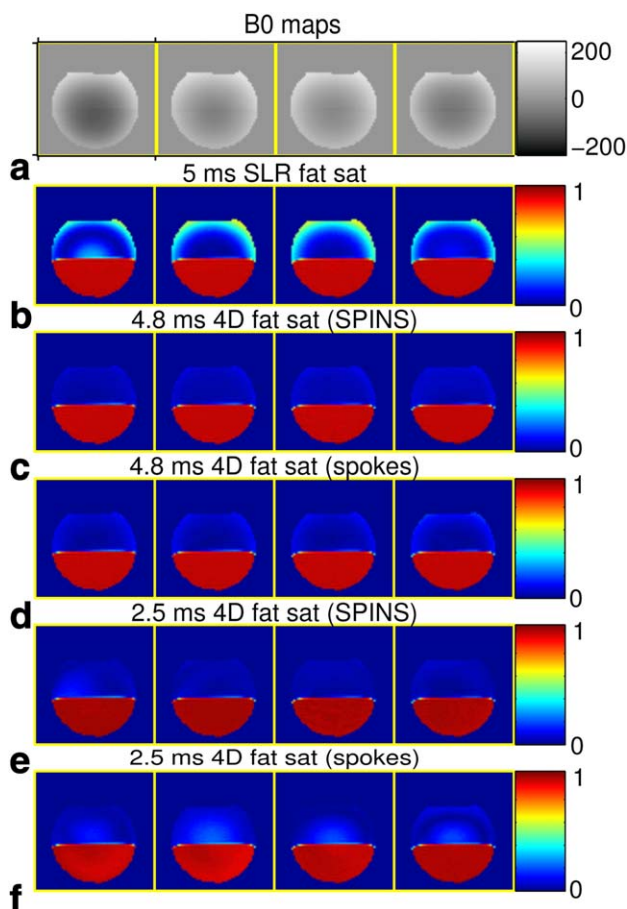
FIG. 6. The B_0 maps and the results of experiment 2, where every third of the axial slices is shown. **a:** The B_0 maps (in Hz); **b–f:** the ratio images by different pulses: (b) 5 ms SLR fat sat pulse, (c) 4.8 ms 4D fat sat pulse with SPINS trajectory or (d) spoke trajectory, (e) 2.5 ms 4D fat sat pulse with SPINS trajectory or (f) spoke trajectory. The ratio images are still the ratio between the images with fat sat and the ones without fat sat, and oil is still on top of water. [Color figure can be viewed in the online issue, which is available at wileyonlinelibrary.com.]

fat sat pulse. Oil is on top of water in the images, and we show the ratio images mentioned in the Methods section which is approximately the absolute value of the normalized residual M_z after the fat sat pulse. By manually selecting the water and fat parts in the images, we put together the histograms of the residual M_z of water and fat parts by the two pulses in Figure 4b. Compared to the SLR fat sat pulse, the 4D fat sat pulse worked nearly the same or a little better for water but much better for fat. Note that some of the M_z of water is greater than 1, which is physically impossible, and the reasons could be artifacts of the spiral imaging and random data noise.

In experiment 2, we tested and compared the proposed method with four different k-space trajectories, and Figure 5 shows examples of the designed pulses with a spoke or SPINS trajectory. Compared to the spoke trajectory which traverses much faster along k_z, the SPINS trajectory traverses excitation k-space more uniformly and has a smoother and slower transition around the $k_x - k_y - k_z$ center. Hence, the RF power of the SPINS pulse

Table 2
RF Energy and Measured Global SAR in Experiment 2

	RF energy ($G^2\mu s$)	Global SAR (W/kg)
5 ms SLR pulse	1.1	0.2
4.8 ms SPINS	9.0	0.4
4.8 ms spokes	11.3	0.4
2.5 ms SPINS	30.5	0.9
2.5 ms spokes	49.3	1.4
no fat sat		0.2

varies less over time and has smaller peak RF power and average power deposition for a given flip angle and pulse length, compared to the spoke pulse. The total RF energy of each pulse, which has been suggested as a surrogate for measuring relative global SAR (30), was calculated using the following formula:

$$E = \int |b(t)|^2 dt \qquad [6]$$

The results of the four 4D fat sat pulses and the SLR fat sat pulse are summarized in Table 2. We also recorded the global SAR of the sequences used in the experiment from the scanner console under a relatively extreme condition, i.e., T_R of the 3D SPGR sequence was set to be the minimum (13 ms), the results of which are also shown in Table 2. Subtracting SAR of the sequence with no fat sat from the other SAR values in Table 2 yields the SAR values induced only by the fat sat pulses, and the values turn out to be roughly proportional to the calculated RF energy values. As expected, the 4D fat sat pulses has much more power than the SLR fat sat pulse, the shorter 4D fat sat pulses induced more SAR than the longer ones, and the SPINS pulses have lower power than the spoke pulses. Although the density of the RF pulses was almost set to be the highest possible, the global SAR is still far below the relevant limit.

As in experiment 1, the ratio images (every third slice) produced by the five different sequences are shown in Figure 6, where fat is still on top of water. To highlight the differences in the fat parts, we show the ratio images in color. The mean and the standard deviation of manually selected fat and water parts in each set of ratio images are shown in Table 3. All the pulses kept the water signal very well, but the 4D fat sat pulses worked much better than the SLR fat sat pulse in the fat part in the presence of B_0 inhomogeneity (Fig. 6). Both of the 4.8 ms 4D fat sat pulses worked very well, and the SPINS pulse is a little better in fat as shown in Figure 6

Table 3
Statistics of Experiment 2

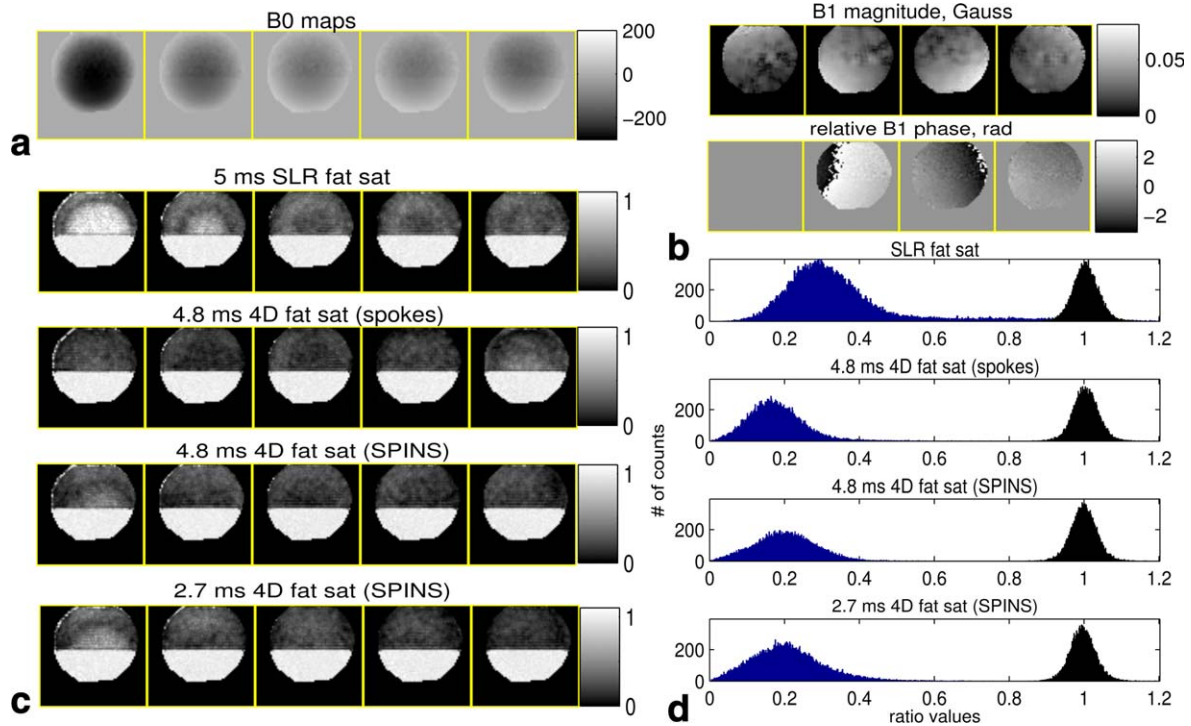|	Mean of ratios (fat)	Std of ratios (fat)	Mean of ratios (water)	Std of ratios (water)
5 ms SLR	0.220	0.16	0.974	0.010
4.8 ms SPINS	0.0532	0.024	0.974	0.0077
4.8 ms spokes	0.0598	0.037	0.975	0.0079
2.5 ms SPINS	0.0483	0.040	1.00	0.0084
2.5 ms spokes	0.0784	0.051	0.982	0.018

FIG. 7. The B_0/B_1 maps and the results of experiment 3. **a:** The B_0 maps (in Hz), where every sixth of the axial slices is shown. **b:** The four-channel B_1 magnitude (top) and relative phase (bottom) of a 2D slice. **c:** The ratio images corresponding to (a) by different pulses; first row: 5 ms SLR fat sat pulse; second row: 4.8 ms 4D fat sat pulse with spoke trajectory; third row: 4.8 ms 4D fat sat pulse with SPINS trajectory; fourth row: 2.7 ms 4D fat sat pulse with SPINS trajectory; The ratio images are still the ratio between the images with fat sat and the ones without fat sat, and oil is still on top of water. **d:** The histograms of the water (black, 200 bins) and fat (blue, 500 bins) M_z according to the ratio images of all the slices. [Color figure can be viewed in the online issue, which is available at wileyonlinelibrary.com.]
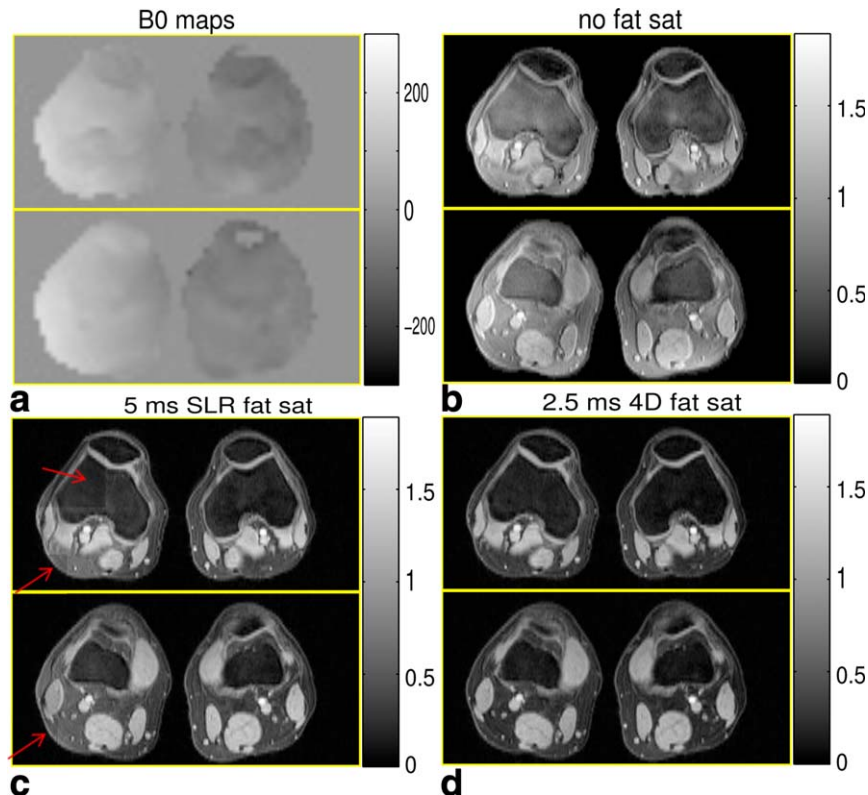

FIG. 8. The B_0 maps and results of the knee imaging, where two representative axial slices are shown. **a:** The B_0 maps (in Hz). **b:** The images without fat sat. **c:** The images with 5 ms SLR fat sat pulse. **d:** The images with 2.5 ms 4D fat sat pulse. [Color figure can be viewed in the online issue, which is available at wileyonlinelibrary.com.]

and Table 3. In contrast, the 2.5 ms SPINS pulse worked much better than the 2.5 ms spoke pulse. Compared to the 4.8 ms SPINS pulse, the 2.5 ms SPINS pulse worked similarly in terms of overall performance; specifically, it has better mean values in both fat and water but bigger variation in the fat part than the 4.8 ms SPINS pulse (Table 3). As SAR may not be an issue here, we think the 2.5 ms SPINS pulse is the best choice for single channel excitation studies in terms of pulse length and overall performance.

Phantom Experiments with Parallel Excitation

Similar to the previous phantom experiments, we calculated the ratio images produced by the four different parallel excitation pulses mentioned in Methods section. Every sixth of the 26 axial images and their corresponding field maps are displayed in Figure 7. By manually selecting the fat and water parts, the histograms of water and fat parts in the ratio images are shown in Figure 7d. As can be seen, the spoke trajectories still suppressed fat much more robustly than the SLR fat sat pulses in the presence of both B_0 and B_1 inhomogeneity, and all of them worked similarly for water. Due to lower signal-to-noise ratio of the parallel excitation system, there are more ratio values in the water part that are greater than 1, compared to the single channel excitation experiments. Comparing the three 4D fat sat pulses, the 4.8 ms spoke pulse worked the best; the overall performance of the two SPINS trajectories is similar, but the 2.7 ms SPINS pulse worked less robustly in the first few axial slices, one of which is shown in the first column of Figure 7c.

In Vivo Experiments with Single Channel Excitation

The results of experiment 4 are shown in Figure 8, where we display two representative axial slices. Compared to the images without fat sat, both fat suppressed images suppressed the fat inside the marrow, and the 4D fat sat pulse worked slightly better. For the fat outside the bones and muscles where B_0 field is more inhomogeneous, the 2.5 ms 4D fat sat pulse worked much better than the 5 ms SLR fat sat pulse.

DISCUSSION

The proposed 4D SPSP fat sat pulse has been demonstrated in various 3T scanner experiments that it can more robustly suppress fat signals with a similar or shorter pulse length in the presence of B_0 and B_1 inhomogeneity compared to the conventional SLR fat sat pulse.

Using the spatial information, the proposed method formulates the fat sat problem as a 4D SPSP problem, which seems more complicated but in fact is quite sensible, as the conventional spectral pulse is generally inefficient for fat sat problems: (a) in fact, the SLR fat sat pulse oversamples k_f (time) domain which, for example, only needs sampling about every 1 ms at 3T, so it has a lot of idle time between the necessary samples, which is efficiently used to handle the spatial variations in the 4D fat sat pulse. (b) The spectral domain problem is easier

when the spatial domain is exploited, as much smaller spatial variations of center frequencies need to be accommodated in the 4D fat sat design, which can largely reduce the pulse length; this is also true when the B_0/B_1 fields are relatively uniform, where not much $k_x - k_y - k_z$ needs to be traversed, and the 4D fat sat pulse will become similar to a SLR fat sat pulse with a very smooth transition band, which can be much shorter than the standard SLR fat sat pulse. On the other hand, when B_0/B_1 fields have large spatial variations, the design requires large $k_x - k_y - k_z$ coverage which is limited by the k_f sampling rate. So as long as the $k_x - k_y - k_z$ coverage can still address the spatial variations, the pulse length will still be as short; otherwise, pulse length will need to be longer, so that a sharper spectral transition band can be obtained to handle the local spatial variations that are not fully compensated by the limited $k_x - k_y - k_z$ coverages.

We assume certain chemical shifts of fat, e.g., 440 Hz at 3T, which could be inaccurate. In fact, such inaccuracy does not affect the result much within a certain range, because the error of chemical shift will be absorbed into the B_0 map acquired with the ΔT_E corresponding to the same inaccurate chemical shift, which only makes the design a little harder due to the discontinuous transitions between water and fat in the B_0 map. In the experimental results, however, there were still some residual fat signals that are higher than simulated. It could be caused by some imperfect system conditions, e.g., nonideal gradient waveforms, inaccurate B_0/B_1 maps, field drift, and inaccurate RF power calibration. In addition, multiple peaks of fat spectrum (25) are not considered in this method, and therefore, some minor fat components can not be suppressed.

We have empirically compared the 4D fat sat pulse with different trajectories in experiment 2 and 3. The SPINS pulses worked better than the spoke pulses in experiment 2 in terms of performance and SAR. However, no clear conclusion can be drawn in experiment 3, because although the spoke pulses gain more efficiency from parallel excitation, they need greater performance penalty in order to satisfy the peak RF power limit. All of the 4D fat sat pulses in experiment 3 were designed with peak RF power penalization. As the SPINS pulse naturally has smaller peak RF power than the spoke pulse, there was less of a performance compromise with the SPINS pulse relative to the spoke pulse. We did not test other spoke trajectories that are shorter than 4.8 ms in experiment 3, because the shorter ones, which need even more RF power, had much poorer performance than the 2.7 ms SPINS trajectory in simulations that penalized RF power. Although the 4.8 ms spoke pulse worked only slightly better than the SPINS trajectories in experiment 3, the spoke trajectories had more advantage in simulations without penalizing peak RF power, including the spoke trajectories shorter than 3 ms. So, as we discussed in Theory section, the spoke pulse with the parallel excitation could work better than the SPINS pulse, but the practical limitations on peak RF power reduce the advantage of the spoke pulse. Moreover, SAR in the parallel excitation experiments, which can not be evaluated by Eq. 6 or global SAR, needs more

investigation, and this may limit the performance of the spoke pulses further. So, the choice of trajectory in the parallel excitation version depends on specific situations. Furthermore, in addition to these empirical experiments where the trajectory parameters were heuristically chosen, more systematic and rigorous studies can be carried out to compare these two trajectories, e.g., pulse design with joint trajectory optimization. Future studies may also include a study of other types of 3D trajectories that are more suitable for this application. One popular 3D trajectory is the stack-of-spiral trajectory (31), but this trajectory can be very inefficient for a nonspatial-selective pulse design like this work. It is efficient for the patterns where in-plane variations dominate, which is generally not the case in the fat sat problem. As the efficiency for traversing $k_x - k_y - k_z$ is very important in our method, stack-of-spiral trajectory will generally be suboptimal compared to the two trajectories used in this article. Another candidate could be the k_T-points trajectory which is an efficient nonselective trajectory for 3D field inhomogeneity compensation (32). This trajectory can be automatically optimized easily and also is able to lower peak RF power and SAR, which are favorable for this 4D fat sat pulse problem.

As shown in the results, the single channel excitation design worked well enough with B_1 inhomogeneity ignored on 3T scanners. In contrast, the parallel excitation pulses worked more poorly than the corresponding single channel excitation pulses, in terms of performance and the required pulse length. Part of the reason is that the custom hardware may have had some imperfections, such as nonlinearity of the RF amplifiers and some eddy current problems, which are being corrected. We only used half of the eight channel system, which may provide little control in some regions between coils. Furthermore, the B_1 maps measured in the experiments may have errors that can be propagated to the pulse design. The B_1 measurements in low magnitude regions may be unreliable, which is a common problem with Bloch-Siegert B_1 mapping. Although we have verified off-line that the B_1 fields of the same phantom along the axial direction were reasonably uniform by looking at the sagittal view B_1 maps, the 3D B_1 maps used in the experiments that were replicas of 2D B_1 maps might still have some variations along axial direction. This can also cause pulse design errors. As the single channel excitation experiments did not compensate for B_1 inhomogeneity, the parallel excitation 4D fat sat pulse may still be advantages in the applications where B_1 inhomogeneity is more problematic, e.g., fat sat in abdominal imaging at 3T (25).

Investigation of the proposed method at different main field strengths could be an interesting future work. At lower field where the pulse length of the conventional fat sat is more problematic, the 4D fat sat pulse could be even more advantageous, because sparser sampling along k_f at lower field allows the 4D fat sat pulse to better compensate for spatial variations which is smaller than at 3T, so that the task in the spectral domain can be simplified even more; in other words, the 4D fat sat pulse length may be shortened further at lower field. In addition, SAR is less of a concern at lower field strength. On the other hand, it will be more challenging to design 4D fat sat pulses at fields higher than 3T where B_0 and B_1 inhomogeneity is more severe. In such designs, the required shorter sampling interval along k_f leaves smaller room for the pulse to compensate for the even larger spatial variations, and parallel excitation will probably be required. Because the pulse length of the conventional fat sat is less of an issue at high field, the proposed method will mainly help to compensate for the field inhomogeneities rather than to shorten the pulse length. We have done some simulation studies on 7T 4D fat sat pulse design which showed some promising results, but SAR may be more problematic.

CONCLUSIONS

We proposed an efficient 4D SPSP fat sat pulse that uniformly suppresses fat without exciting water in the presence of B_0 and B_1 inhomogeneity with single channel or parallel excitation system. In the 3T experiments, the proposed method showed superior performance in terms of fat suppression and pulse length compared to the SLR fat sat pulse. In particular, the proposed pulse was only half of the standard fat sat pulse in the single channel excitation experiments. We also found that the SPINS trajectory is generally preferred to spoke trajectory in single channel excitation, but the choice of trajectory in parallel excitation depends on specific situations. This approach must be very useful in a variety of applications at different field strengths.

REFERENCES

1. Haase A, Frahm J, Hanicke W, Matthaei D. 1h NMR chemical shift selective (chess) imaging. Phys Med Biol 1985;30:341–344.
2. Delfaut E, Beltran J, Johnson G, Rousseau J, Marchandise X, Cotten A. Fat suppression in MR imaging: techniques and pitfalls. Radiographics 1999;19:373–382.
3. Tien R. Fat-suppression MR imaging in neuroradiology: techniques and clinical application. Am J Roentgenol 1992;158:369–379.
4. Meyer C, Pauly J, Macovskiand A, Nishimura D. Simultaneous spatial and spectral selective excitation. Magn Reson Med 1990;15:287–304.
5. Morrell G, Macovski A. Three-dimensional spectral-spatial excitation. Magn Reson Med 1997;37:378–386.
6. Heilman JA, Derakhshan JD, Riffe MJ, Gudino N, Tkach J, Flask CA, Duerk JL, Griswold MA. Parallel excitation for b-field insensitive fat-saturation preparation. Magn Reson Med 2012;68:631–638.
7. Setsompop K, Alagappan V, Gagoski B, Potthast A, Hebrank F, Fontius U, Schmitt F, Wald L, Adalsteinsson E. Broadband slab selection with b 1+ mitigation at 7t via parallel spectral-spatial excitation. Magn Reson Med 2009;61:493–500.
8. Malik S, Larkman D, O'Regan D, Hajnal J. Subject-specific water-selective imaging using parallel transmission. Magn Reson Med 2010; 63:988–997.

9. Grissom W, Yip C, Zhang Z, Stenger V, Fessler J, Noll D. Spatial domain method for the design of RF pulses in multicoil parallel excitation. Magn Reson Med 2006;56:620–629.

10. Setsompop K, Wald L, Alagappan V, Gagoski B, Adalsteinsson E. Magnitude least squares optimization for parallel radio frequency excitation design demonstrated at 7 tesla with eight channels. Magn Reson Med 2008;59:908–915.

11. Kassakian P. Convex approximation and optimization with applications in magnitude filter design and radiation pattern synthesis. Berkeley: University of California; 2006.

12. Fessler JA, Sutton BP. Nonuniform fast fourier transforms using min-max interpolation. IEEE Trans Signal Process 2003;51:560–574.

13. Saekho S, Yip C, Noll D, Boada F, Stenger V. Fast-kz three-dimensional tailored radiofrequency pulse for reduced B1 inhomogeneity. Magn Reson Med 2006;55:719–724.

14. Malik SJ, Keihaninejad S, Hammers A, Hajnal JV. Tailored excitation in 3D with spiral nonselective (spins) RF pulses. Magn Reson Med 2012;67:1303–1315.

15. Zelinski AC, Wald LL, Setsompop K, Goyal VK, Adalsteinsson E. Sparsity-enforced slice-selective MRI RF excitation pulse design. IEEE Trans Med Imaging 2008;27:1213.

16. Ma C, Xu D, King KF, Liang ZP. Joint design of spoke trajectories and RF pulses for parallel excitation. Magn Reson Med 2011;65:973–985.

17. Yoon D, Fessler JA, Gilbert AC, Noll DC. Fast joint design method for parallel excitation radiofrequency pulse and gradient waveforms considering off-resonance. Magn Reson Med 2012;68:278–285.

18. Grissom WA, Khalighi MM, Sacolick LI, Rutt BK, Vogel MW. Small-tip-angle spokes pulse design using interleaved greedy and local optimization methods. Magn Reson Med 2012;68:1553–1562.

19. Grissom W, Yip C, Wright S, Fessler J, Noll D. Additive angle method for fast large-tip-angle rf pulse design in parallel excitation. Magn Reson Med 2008;59:779–787.

20. Xu D, King K, Zhu Y, McKinnon G, Liang Z. Designing multichannel, multidimensional, arbitrary flip angle RF pulses using an optimal control approach. Magn Reson Med 2008;59:547–560.

21. Grissom W, Xu D, Kerr A, Fessler J, Noll D. Fast large-tip-angle multidimensional and parallel RF pulse design in MRI. IEEE Trans Med Imaging 2009;28:1548–1559.

22. Hollingsworth N, Moody K, Nielsen J, Noll D, McDougall M, Wright S. Tuning ultra-low output impedance amplifiers for optimal power and decoupling in parallel transmit MRI. In IEEE International Symposium on Biomedical Imaging: From Nano to Macro, San Francisco, 2013;946–949.

23. Moody KL, Hollingsworth NA, Nielsen JF, Noll D, McDougall MP, Wright SM. Eight-channel transmit/receive head array for use with ultra-low output impedance amplifiers. In IEEE International Symposium on Biomedical Imaging: From Nano to Macro, San Francisco, 2013;950–953.

24. Pauly J, Le Roux P, Nishimura D, Macovski A. Parameter relations for the Shinnar-Le Roux selective excitation pulse design algorithm [NMR imaging]. IEEE Trans Med Imaging 1991;10:53–65.

25. Bley TA, Wieben O, François CJ, Brittain JH, Reeder SB. Fat and water magnetic resonance imaging. J Magn Reson Imaging 2010;31:4–18.

26. Sacolick L, Wiesinger F, Hancu I, Vogel M. B1 mapping by Bloch-Siegert shift. Magn Reson Med 2010;63:1315–1322.

27. Zhao F, Fessler J, Nielsen JF, Noll D. Regularized estimation of magnitude and phase of multiple-coil B1 field via Bloch-Siegert B1 mapping. In Proceedings of the 20th Scientific Meeting of International Society for Magnetic Resonance in Medicine, Melbourne. 2012; p. 2512 .

28. Zhao F, Fessler JA, Wright SM, Rispoli JV, Noll DC. Optimized linear combinations of channels for complex multiple-coil B1 field estimation with Bloch-Siegert B1 mapping in MRI. In IEEE International Symposium on. Biomedical Imaging: From Nano to Macro, San Francisco, 2013. p. 942.

29. Collins C, Liu W, Swift B, Smith M. Combination of optimized transmit arrays and some receive array reconstruction methods can yield homogeneous images at very high frequencies. Magn Reson Med 2005;54:1327–1332.

30. Bardati F, Borrani A, Gerardino A, Lovisolo G. Sar optimization in a phased array radiofrequency hyperthermia system. IEEE Trans Biomed Eng 1995;42:1201–1207.

31. Saekho S, Boada FE, Noll DC, Stenger VA. Small tip angle three-dimensional tailored radiofrequency slab-select pulse for reduced b1 inhomogeneity at 3 T. Magn Reson Med 2005;53:479–484.

32. Cloos M, Boulant N, Luong M, Ferrand G, Giacomini E, Le Bihan D, Amadon A. kt-points: short three-dimensional tailored RF pulses for flip-angle homogenization over an extended volume. Magn Reson Med 2012;67:72–80.